

Dissipation in the Magnetic Turbulence of Reversed Field Pinch Plasmas

J. B. Titus,^{1,2, a)} A. F. Almagri,³ P. W. Terry,³ J. S. Sarff,³ E. Mezonlin,¹ and J. A. Johnson, III^{1, b)}

¹⁾Florida A&M University, Tallahassee, Florida 32307, USA

²⁾TAE Technologies, Inc., Foothill Ranch, California 92610, USA

³⁾University of Wisconsin-Madison, Madison, Wisconsin 53706, USA

(Dated: 29 May 2021)

Reversed field pinch plasmas are subject to tearing instability that creates a broad spectrum of magnetic fluctuations. The dominant fluctuations have poloidal and toroidal mode numbers $(m, n) = (1, 6 - 10)$ and can grow to 2 - 3% of the mean magnetic field. Through non-linear coupling this growth culminates in a strong reconnection event and broadening of the magnetic spectrum extending to the ion gyroradius scale. Multiple developments occur during the reconnection stage: ions and electrons are energized, magnetic fluctuation amplitudes increase, plasma flow is halted, and the toroidal magnetic flux increases in a sawtooth-like fashion as the RFP dynamo becomes stronger. Magnetic fluctuations are measured in the plasma edge at multiple radial locations from $r/a = 0.75$ to 0.96 to assess and characterize the magnetic turbulence. The measured spectrum perpendicular to the mean field, $S(k_{\perp})$, can be fit to a model spectrum consisting of power law and exponential component with one free parameter that characterizes dissipation. The measured dissipation is much larger than estimated from classical viscous or resistive dissipation, but it is consistent with a flow damping measurement of anomalous viscosity. The measurements show an evolution of the spectrum during which fluctuation power builds up in the smallest wavenumbers and cascades to the larger wavenumber due to the non-linear coupling between the linear $(m, n) = (1, > 6)$ and the non-linear $(m, n) = (0, 1)$ tearing modes.

I. INTRODUCTION

Magnetic turbulence occurs in many astrophysical and laboratory plasmas and is fundamental to many plasma processes.²⁻⁴ Some of these mechanisms include the conversion of plasma flow into magnetic energy and conversion of magnetic energy to thermal energy.^{5,6} Magnetic turbulence also plays an important role in the transport of particles, energy, and momentum.⁷ Often the turbulence is characterized by a broadband spectrum exhibiting a power-law dependence on wavenumber and/or frequency indicative of an energy conserving cascade of turbulent energy from large scale to small scale. In some cases, as observed in the aurora and solar wind,^{3,8,9} the measured magnetic power spectra have two power-law zones in the wavenumber. Power in the high wavenumber zone falls off more steeply, having a larger spectral index than the falloff in the low wavenumber zone, and creating a qualitative “break” in the spectra. The increased spectral index is possibly associated with the onset or enhancement of dissipation that removes energy from the turbulence. In Navier-Stokes turbulence, the transition to the dissipation range begins at the Kolmogorov scale and leads to exponential falloff with increasing wavenumber, which can be represented by multiple power-laws with increasing spectral indices. When dissipation occurs over a range of scales, it is appropriate to characterize the spectrum as the product of exponential and power-law dependencies.

Laboratory plasma experiments provide a complementary setting for investigations of magnetized plasma turbulence. They overcome some of the limitations of spacecraft measurements¹⁰ by allowing highly repeatable measurements of magnetic fluctuation at many locations, digitized with high

frequency bandwidth and high signal-to-noise resolution. For example, reversed field pinch (RFP) plasmas exhibit a well-developed magnetic turbulent cascade.¹¹ The RFP is a toroidal plasma confinement configuration that is magnetized primarily by current in the plasma rather than external magnets. Several large-scale tearing modes are destabilized by a centrally peaked inductive current profile and nonlinearly couple to stable modes, energizing a broad spectrum that cascades energy to at least the ion gyroradius scale. The magnetic turbulence is anisotropic relative to the confining magnetic field, i.e., broad (narrow) in the perpendicular (parallel) direction relative to the local mean magnetic field. Short wavelength fluctuations exhibit exponential falloff indicative of dissipation.¹² The turbulent kinetic energy is smaller than the magnetic energy at large scale, consistent with tearing instability, but the kinetic energy exceeds the magnetic energy at intermediate and small scales. The fluctuation characteristics at these scales are consistent with the appearance of drift waves in the cascade, excited either nonlinearly or through micro-instability associated with the large pressure gradient near the plasma boundary.¹³

The RFP plasma also exhibits distinct, quasi-periodic magnetic reconnection¹⁴ events in the multiple helicity regime (MH).¹⁵ These events are related to the nonlinear saturation process for tearing instability, suppressing toroidal plasma current in the core and sustaining poloidal plasma current near the toroidal field reversal surface (referred to as the RFP dynamo process). The tearing fluctuations increase during each of these events, impulsively energizing the turbulent cascade.^{12,16,17} Motivated by these and several other observations, theoretical work has been performed to develop a visco-resistive dissipation-range magneto hydrodynamic (MHD) model. Under multiple closure schemes, the theoretical energy spectrum is:

$$E(k) = a\varepsilon^{2/3}k^{-5/3} \exp \left[-b \left(\frac{k}{k_d} \right)^{\alpha} \right], \quad (1)$$

^{a)}Electronic mail: jtitus@tae.com

^{b)}Deceased, June 25, 2017.

where ε is the energy input rate, a and b are constants, and α falls between 1 and 2 (depending on the closure).¹⁸ The parameter k_d sets the characteristic scale for the onset of dissipation. This spectral representation of the turbulent cascade is suitable for characterizing the rate at which energy cascades from scale to scale and for indicating where the dissipation rate dominates the eddy turnover rate. The latter defines the dissipation range where kinetic energy is converted to thermal energy.

Non-collisional ion heating and particle energization are commonly observed in turbulent plasmas. These processes are especially powerful in RFP plasmas, and the ion temperature can exceed the electron temperature, $T_i > T_e$. Energetic tails form spontaneously for both ions and electrons. As much as 10 - 30% of the plasma's stored magnetic energy, $E_{mag} = \int B^2 dV / 2\mu_0$, is released during a sawtooth magnetic reconnection event, but a large portion of this energy remains confined as ion thermal energy. The ion heating efficiency scales with the square root of the mass of the bulk ion species,⁶ and impurity (minority) ions attain temperatures exceeding the bulk ion temperature.¹⁹ There is also a charge to mass ratio dependence.²⁰ While the heating occurs globally within the plasma, the local temperature correlates with 3D magnetic structure.²¹ A non-Maxwellian tail forms in the perpendicular ion energy distribution function during the sawtooth crash,²²⁻²⁴ where the ratio of fast ions to bulk ions increases with increasing E_{mag} .²⁵ In addition, while electron temperatures show little sign of increasing during magnetic reconnection events, there is evidence of anisotropic electron-tail generation.²⁶

In this paper, we characterize the dissipation in the magnetic turbulence of MST RFP plasmas through a set of probe measurements made in the outer region of the plasma. The spectra are well represented by Eq. 1 throughout the edge region. The best-fit values for k_d are much smaller than expected for collisional dissipation, suggesting a close relationship to ion heating and particle energization. We also show that the transient associated with a sawtooth magnetic reconnection event initially energizes the long wavelength portion of the turbulent spectrum, consistent with the canonical picture for a cascade driven by large-scale instability.

II. EXPERIMENTAL SETUP

The MST is an axisymmetric toroidal plasma device with a major radius of 1.5 m and minor radius of 0.52 m.¹ It typically operates in the reversed-field configuration (RFP), where magnetic fields are generated mostly from plasma currents. In this regime, MST produces plasma currents between 75 to 600 kA, with electron temperatures $T_e > 1$ keV, electron densities $n_e \sim 0.5 - 1.3 \times 10^{13} \text{ cm}^{-3}$, and a plasma beta near 10%.²⁷ Low-current 200 kA plasmas are studied here, which are amenable to insertable probes. A study was completed with different sized particle shields in similar conditions. The different sized shields had negligible effect to the magnetic fluctuation measurements.

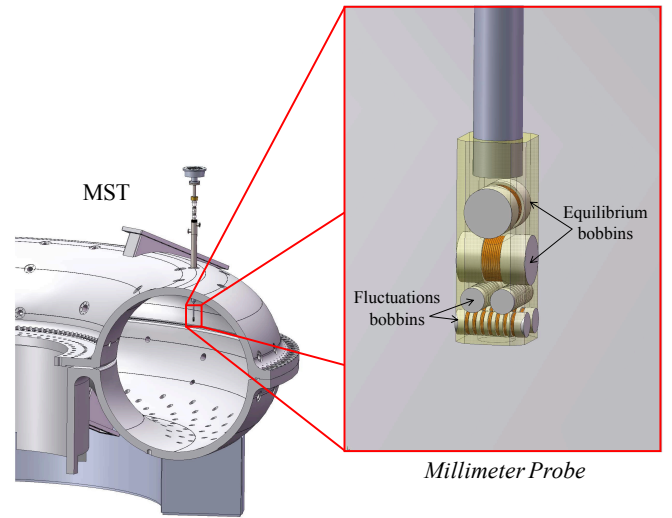


FIG. 1. The millimeter probe is shown at the entrance into MST. There are six bobbins containing magnetic pickup coils, which are protected by a boron-nitride shield. The two large bobbins are intended for equilibrium measurements, and four smaller bobbins contain seven slots intended for fluctuation measurements. The probe was inserted into MST in the radial direction to sample magnetic fluctuations at the plasma edge. [Associated dataset available at <http://dx.doi.org/10.5281/zenodo.4455538>] (Ref. 29).

In the RFP configuration, parallel currents create a sheared equilibrium magnetic field and current density gradient. This allows tearing mode resonances, (m, n) , having poloidal and toroidal mode numbers, $(m = 1, n \gtrsim 2R = a)$, as well as $(m = 0, n \geq 1)$. Several of the innermost-resonant $m = 1$ modes are linearly unstable, and nonlinear coupling energizes a broad spectrum with resonant surfaces throughout the plasma volume. Global nonlinear coupling is facilitated especially by $m = 0$ modes¹⁶ that are resonant at the toroidal magnetic field reversal surface, where the mean magnetic field is pointing in the poloidal direction and the toroidal component is zero. When the $m = 0$ amplitude reaches a critical value, global magnetic reconnection occurs, abruptly releasing a large amount of magnetic energy and flattening the current density gradient. As current continues to be driven, this sequence repeats quasi-periodically in a sawtooth cycle. The amplitudes of magnetic fluctuations burst at each sawtooth "crash" event, turbulent particle and energy is enhanced, and powerful non-collisional ion heating is produced.

The novel probe, shown in Fig. 1, was designed to measure magnetic equilibrium and fluctuations in the toroidal T and poloidal P directions with high spatial and frequency resolution, $B_{T,P}$ and $\dot{B}_{T,P}$. This is dubbed the *millimeter probe*. There are six bobbins containing magnetic pickup coils, which are protected from plasma energetic particles and heat by a boron-nitride shield, and from electrostatic fields by a microscopic layer of silver. The two large bobbins are wound with two layers of 20 total turns of 32 AWG wire, which are intended for equilibrium measurements of the mean magnetic field components. The four smaller bobbins each contain seven slots separated by 0.1 cm; each slot is wound

with two layers of four total turns of 36 AWG wire. These coils with low inductance are intended for high frequency fluctuation measurements. Each set of two parallel bobbins are separated by 0.4 cm and oriented to measure magnetic fluctuations in the poloidal and toroidal direction. Magnetic signals are sampled at 6 MHz with an instrumental bandwidth 3.0 MHz. The equilibrium coils are actively integrated.

Multiple $dB_{T,P}/dt$ measurements from the millimeter probe are used to calculate multiple unique magnetic field power spectral densities as a function of wavenumber and frequency, $S(k_P, k_T, f)_i$, where i is the iteration of each unique power spectral density. The spectra are calculated using the two-point correlation technique.²⁸ Even though coils on the same bobbin are only separated by 0.1 cm, $S(k_P, k_T, f)_i$ is limited to 0.4 cm because of the separation of parallel bobbins. From two bobbins that are oriented to measure the toroidal component of the magnetic field, four coils that are located at the four corners of a square of 0.4 cm on a side are selected to calculate $S(k_P, k_T, f)_i$. For example, one measurement of $S(k_P, k_T, f)_i$ can be calculated from the cross-correlation of measurements from the 1st and 5th coils in bobbin 1 and the cross-correlation of measurements from the 1st coils from bobbin 1 and 2. There are a possible 24 coil combinations, creating 24 unique $S(k_T, k_P, f)_i$ from the millimeter probe measurements.

Characterizing the dissipation in the wavenumber spectrum perpendicular to the mean magnetic field, $S(k_\perp)$, is the primary focus of this study. The perpendicular and parallel spectral densities, $S(k_\perp)_i$ and $S(k_\parallel)_i$, are obtained from integrating in frequency-space up to the frequency at which coherence between coils becomes poor (~ 800 kHz): $S(k_T, k_P)_i = \int S(k_T, k_P, f)_i df$, using the vector relationship $k_\parallel = (k_P B_P + k_T B_T)/B$ and $k_\perp = (k_T B_P - k_P B_T)/B$ where $B = \sqrt{B_T^2 + B_P^2}$. Then $S(k_\perp)_i = \int S(k_\parallel, k_\perp)_i dk_\parallel$. For this study, we only used $S(k_T, k_P)_i$ from the two bobbins closest to the equilibrium coils (12 total). The 12 $S(k_\perp)_i$ measurements are then averaged together to create one refined $S(k_\perp)$.

The probe was inserted into MST plasmas in the radial direction to sample magnetic fluctuations in MH, deuterium plasmas at different depths from $r/a = 0.79$ to 0.95. This range covers the edge of the plasma from the limiter to the toroidal magnetic field reversal-surface. There are strong gradients in the equilibrium plasma temperature and density in this region.³⁰ The plasma current of these discharges was ~ 200 kA, with a line-average electron density of $n_e \sim 1.0 \times 10^{13} \text{ cm}^{-3}$, a core electron temperature of $T_0 \sim 180$ eV, and a reversal parameter of $F = B_{tor}(a)/\langle B_{tor} \rangle = -0.2$, where $\langle B_{tor} \rangle$ is the volume-average toroidal field. One hundred discharges were created for each radial position, leading to ~ 300 global magnetic reconnection events for each position.

III. FLUCTUATION MEASUREMENTS AND POWER SPECTRA, $S(k_\perp)$

During the sawtooth relaxation cycle in MST plasmas, magnetic fluctuations spike due to enhanced current-gradient

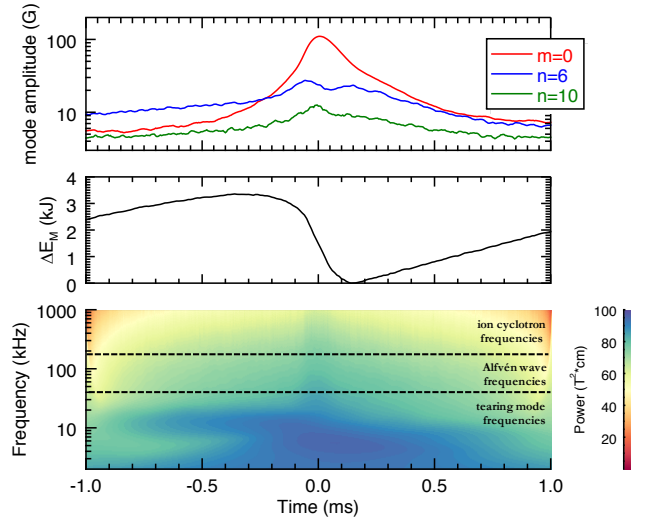


FIG. 2. Ensemble averaged measurements during magnetic reconnection in MST plasmas. a) $(m, n) = (0, 1)$, $(m, n) = (1, 6)$ and $(m, n) = (1, 10)$ tearing modes; b.) total stored magnetic energy in the plasma; c.) spectrogram of Morlet wavelet with power from a coil near the edge of the plasma. Characteristic frequency bands for tearing mode, Alfvén waves, and ion cyclotron frequencies are indicated by dotted lines. [Associated dataset available at <http://dx.doi.org/10.5281/zenodo.4455538>] (Ref. 29).

driven tearing-mode instability and subsequent changes to the magnetic field configuration. An ensemble of a large number of sawtooth cycles is shown in Fig. 2, where ensembled sawtooth events with a 2 ms window are centered at $t = 0$, corresponding to the maximum of the $(m, n) = (0, 1)$ amplitude. Dominant tearing-mode amplitudes and stored magnetic energy in the equilibrium field are shown in Figs. 2a and 2b. A Morlet wavelet spectrogram of magnetic field fluctuations is shown in Fig. 2c, where the measurements are from a magnetic pickup coil in the millimeter probe at the insertion depth of $r/a = 0.81$. Characteristic frequency bands for tearing mode, Alfvén waves, and ion cyclotron frequencies are indicated by dotted lines.

In Fig. 2a the core-resonant tearing modes with $(m, n) = (1, 6)$ and $(1, 10)$ begin to grow above their nominal steady state value at $t \sim -1$ ms, indicating the start of the sawtooth cycle. The stored magnetic energy begins increasing around the same time, as does fluctuating power in the 10 - 20 kHz tearing-mode range. The increase in levels of the $(m, n) = (1, 6)$ and $(1, 10)$ and $(m, n) = (0, 1)$ fluctuations around -0.5 ms indicate an onset of significant non-linear activity. The $(m, n) = (0, 1)$, which is generally linearly stable, is non-linearly driven in the sawtooth cycle, and enables non-linear coupling to $m = 1$ modes with higher n number.^{16,31} The stored magnetic energy begins to decrease as the amplitude of $(m, n) = (0, 1)$ increases. Around -0.1 ms, magnetic fluctuation power becomes more broadband as energy in the Alfvén frequency range (50 - 200 kHz) and ion cyclotron frequency range (200 - 600 kHz) increases. Note that the stored magnetic energy drops precipitously around $t = 0$ as the spectrum broadens,

consistent with a cascade driven by magnetic reconnection from unstable tearing.¹² When the tearing mode amplitudes subside, the crash phase ends, and the cycle repeats.

Energy released into the turbulent cascade is ultimately removed from the spectrum in some form of dissipation. Possible dissipation mechanisms include collisions, manifest as fluid resistivity and viscosity, collisionless processes, e.g., gyroviscosity expressed in a fluid formalism, and intrinsically kinetic processes, like Landau damping or ion-cyclotron resonance damping. Fluctuations affect these processes, for example raising the rate of dissipation if fluctuations are sheet like and therefore favorable for magnetic reconnection. Fluctuations also affect mean quantities through transport and can give rise to anomalous diffusivities, which may or may not extract energy from a cascade. The characteristic scaling of the turbulent cascade provides insight into dissipation as revealed in the exponential tail of the wavenumber spectra, which is a major theme for this paper.^{18,32}

Prior measurements have shown that the magnetic turbulence in RFP plasmas is highly anisotropic with more energy in wavenumbers perpendicular to the equilibrium magnetic field. The propagation is also asymmetric, favoring the electron diamagnetic drift direction. The perpendicular wavenumber spectrum, $S(k_{\perp})$, contains an exponential component in addition to a power-law feature.¹² The spectrum was fitted to the general form:

$$S(k_{\perp}) \sim k_{\perp}^{-\alpha} \exp[-\beta(k_{\perp}/k_d)^{\gamma}], \quad (2)$$

with determined values of α , β , and γ given by $5/3$, $3/2$, $4/3$, respectively, and k_d as a free parameter. The parameter k_d corresponds to the Kolmogorov wavenumber in hydrodynamic turbulence and identifies the wavenumber above which the dissipation rate exceeds the eddy turnover rate and the spectrum begins to exponentially decay. The best fit of $S(k_{\perp})$ to the data at $r/a \sim 0.81$ yielded $k_d = 0.85 \text{ cm}^{-1}$.¹⁸

When the non-linear interaction is its strongest ($-0.175 < t < 0.175$ ms), increases in fluctuation power are mostly perpendicular to the equilibrium magnetic field. It has been recognized for some time that the perpendicular wavenumber spectrum $S(k_{\perp})$ in the electron diamagnetic direction develops an exponential component in addition to the traditional power-law feature.¹² The spectrum $S(k_{\perp})$ at $r/a \sim 0.81$ is measured with the millimeter probe and fit to Eq. 2, with the previously determined values and free parameter. As shown in Fig. 3 the spectrum has an exponential feature, indicating that dissipation is important in the spectrum. The best fit of $S(k_{\perp})$ to MST data at $r/a \sim 0.81$ yields $k_d = 0.85 \text{ cm}^{-1}$, indicating that the dissipation rate dominates the non-linear decorrelation rate for $k > 0.85 \text{ cm}^{-1}$. This result is consistent with previous measurements,¹² demonstrating the robustness of this phenomenon in the plasma and the measurements. The development of dissipation in this wavenumber range correlates temporally with the magnetic energy loss and its associated processes, but its spatial characteristics are not well understood. This paper seeks to better characterize the dissipation-range spectrum.

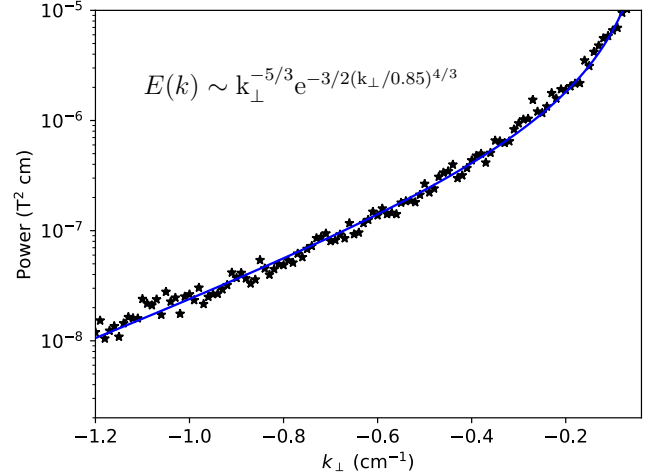


FIG. 3. The k_{\perp} power spectrum in the electron-diamagnetic direction at $r/a = 0.81$, fit with Eq. (1). The values for α , β , and γ were by $5/3$, $3/2$, $4/3$, respectively, and k_d was used as the fitting parameter. [Associated dataset available at <http://dx.doi.org/10.5281/zenodo.4455538>] (Ref. 29).

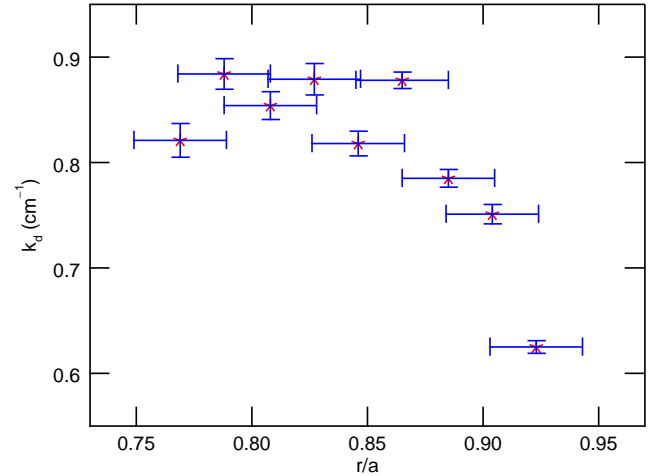


FIG. 4. The calculated Kolmogorov wavenumber, k_d , at each insertion depth. The r/a error bars show the extent of the coil locations in the probe and the k_d error bars are from the fit uncertainty. [Associated dataset available at <http://dx.doi.org/10.5281/zenodo.4455538>] (Ref. 29).

IV. SPECTRUM CHARACTERIZATION

A. k_d and the Origin of Dissipation

If k_d arises from classical resistivity in $\text{Pm} < 1$ MHD turbulence, it is given by $k_d = (\varepsilon/\eta^3)^{1/4}$, where $\text{Pm} = \mu/\eta$ is the magnetic Prandtl number, μ is the viscosity, η is the resistiv-

ity, and ε is the rate energy is injected into turbulent fluctuations. Because $k_d \sim \eta^{-3/4}$ and $\eta \sim T_e^{-3/2}$, k_d is dominated by the direct resistivity dependence and expected to scale with the electron temperature $k_d \sim T_e^\lambda$, with $\lambda = 9/8$. Figure 4 shows the best-fit k_d from the probe measurements at different spatial locations in the edge region. The r/a error bars show the extent of the coil locations in the probe and the k_d error bars are the from the fit uncertainty. All values are near $k_d \approx 0.85 \text{ cm}^{-1}$, except for $r/a = 0.92$, which may be affected by close proximity to the wall. This region of the plasma has a large temperature gradient, decreasing by $\sim 50\%$,³⁰ over the edge region. For the MST plasmas in this study, the classical resistivity is $\eta \sim 5 \text{ m}^2/\text{s}$ using characteristic values of $T_e = 180 \text{ eV}$ and $Z_{eff} = 2$ for the edge region, which corresponds to a dissipation wavenumber $k_{\eta_{class}} = 3.0 \text{ cm}^{-1}$.

To explore this further, consider the model spectrum,

$$\frac{S(k_\perp)}{\mu_0 \rho} = E(k_\perp) = C_k \varepsilon^{2/3} |k_\perp|^{-5/3} \exp \left[-3/2 \left(\frac{k}{k_d} \right)^{4/3} \right], \quad (3)$$

where ρ is the plasma mass density, C_k is an overall constant known as the Kolmogorov constant in hydrodynamics, and μ_0 is magnetic permeability.³² The exponents are as noted above, given that they provide a good fit to the measured spectra. Let us examine how the spectrum measured in MST compares with predicted spectra when experimentally known values of classical resistivity η and viscosity μ are used to calculate a theoretical value of k_d . This is essentially a comparison exercise of the measured spectrum to known theoretical benchmarks. Aside from providing context for the spectrum, it allows assessment of whether the measured spectrum is sufficiently like a spectrum arising from collisional dissipation processes, indistinguishable within measurement uncertainty. As stated above, $k_d = (\varepsilon/\eta^3)^{1/4}$ for $\text{Pm} < 1$ and resistive dissipation is dominant. Similarly, $k_d = (\varepsilon/\mu^3)^{1/4}$, for $\text{Pm} > 1$ and viscous dissipation is dominant. A modeled spectrum with α , β , and γ as given above, and $k_d = k_{\eta_{class}}$ is plotted as a function of k_\perp in Fig. 5 together with the measured spectrum at $r/a = 0.81$. The characteristic mass density $\rho \sim 1 \times 10^{-8} \text{ kg m}^{-3}$, C_k is assumed to be order unity, and ε was previously measured to be $\sim 2 \times 10^{12} \text{ m}^2 \text{ s}^{-3}$.¹² In similar fashion, the classical (perpendicular) viscosity in MST is dominated by charged particle collisions and has a value of $\mu_{class} = 0.6 \text{ m}^2/\text{s}$ using characteristic edge plasma parameters. This corresponds to $k_{\mu_{class}} = 17.5 \text{ cm}^{-1}$ and places the plasma in the regime $\text{Pm} < 1$. For reference, the model spectrum with $k_d \sim k_{\mu_{class}}$ is also plotted in Fig. 5. Given that this spectrum has an onset of dissipation at a considerably higher wavenumber, it is closer to the pure inertial range power law spectrum with $k_\perp^{-5/3}$.

These comparisons emphasize that classical processes are insufficient to explain the onset of dissipation in the observed turbulent magnetic spectrum. The ion heating observed in MST plasmas, where $T_i \gg T_e$, also requires a process beyond classical dissipation. The ion heating is not only energetic, it is powerful, reaching order 10 MW during the rapid sawtooth crash. Rapid heating via a turbulent cascade requires dissipation at scales having substantial electric field fluctuations.³²

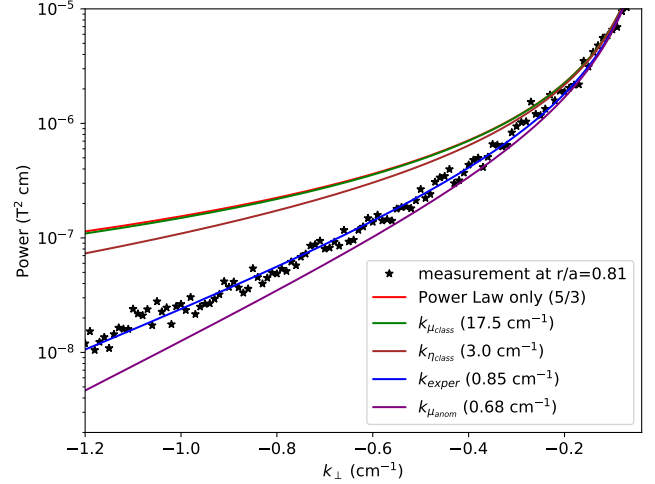


FIG. 5. The k_\perp power spectrum (black stars) is compared to a power-law fit (red line), an exponential + power-law fit (blue line) and several fitted lines using Eq. (1 and distinct values of k_d calculated from: classical resistivity (cyan), classical viscosity (green), and anomalous viscosity (blue). [Associated dataset available at <http://dx.doi.org/10.5281/zenodo.4455538>] (Ref. 29).

The inferred onset of dissipation in the magnetic turbulence at scales larger than expected for collisional processes bolsters the possibility for powerful non-collisional turbulent heating.

There is additional evidence for non-collisional dissipation in previous measurements of flow damping in the edge of similar MST plasmas.³³ A biased electrode inserted in the edge region was used to apply a torque on the plasma, and the relaxation of the flow following rapid turn-off of the bias voltage allowed measurements of the perpendicular viscosity, estimated to be $\mu_{anom} \approx 45 \text{ m}^2/\text{s}$ (subscripted "anom" to indicate it is anomalous relative to the classical value $\mu_{class} = 0.6 \text{ m}^2/\text{s}$ noted above). If this anomalous viscosity is responsible for dissipating power in the fluctuation spectrum, it corresponds to a dissipation wavenumber $k_{anom} = 0.68 \text{ cm}^{-1}$. A model spectrum with $k_d \sim k_{anom}$ is plotted in Fig. 5, which is close to the experimental spectrum. Note that the values for the best-fit $k_d \approx 0.85 \text{ cm}^{-1}$ in Fig. 4 happen to have $k_d \approx k_{anom}$. This is highly suggestive that a non-collisional process is responsible for dissipation of fluctuation power in the spectrum, for the anomalous viscosity, and possibly for non-collisional ion heating. Anomalous viscosity is intrinsic to turbulent fluctuations, which act to scatter momentum. The direct consequence are the Reynolds and Maxwell stresses that arise from the nonlinearities in momentum balances, and through flux-gradient relations give rise to anomalous viscosity. However, it should be noted that anomalous viscosity need not dissipate fluctuation power. Flows could be slowed down by fluctuations that are strictly inertial, in which case an anomalous viscosity would not correspond to a dissipative feature in the spectrum, but rather the conservative energy transfer associated with a power law.

B. The Temporal Evolution of the Spectrum

At the peak of the sawtooth crash, previous measurements indicated increased power at all k_{\perp} in the spectrum.¹² However, those measurements did not indicate how and when this increase occurs. Investigating the spectrum at different time windows during the sawtooth cycle can help characterize different subranges of the k_{\perp} spectrum and provide insight into the dissipation-related time scales. It can also shed light on the nature of the anomalous viscosity.

Figure 6 shows the evolution of the k_{\perp} power spectrum during the sawtooth crash at the $r/a \sim 0.81$ location. The spectra represent distinct 0.35 ms time windows, with the middle window centered at the crash peak. The -1.225 to -0.875 ms spectrum represents "before" the crash. During the -0.875 to -0.525 ms time window (which is not shown in the figure), fluctuations in the lowest wavenumbers ($k < 0.05 \text{ cm}^{-1}$) begin to increase while fluctuations in the larger wavenumbers remain unchanged from the previous time window. This continues during the -0.525 to -0.175 ms time window as well, which is shown in the figure. This indicates there is a separate mechanism that only adds additional power to the smaller wavenumber. During the -0.175 to 0.175 ms time window ("during" the crash), power in all wavenumbers has increased. The three time windows before the peak of the crash suggest that power builds up in the smallest wavenumbers and then cascades down to the larger wavenumbers. This increased power builds up over 0.7 ms and cascades quickly within 0.35 ms, approximately the eddy turnover time for the largest scale tearing modes. This confirms the smallest wavenumbers as the injection source of the cascade. During the 0.175 to 0.525 ms time window, the power in the smallest wavenumbers decreases to "before" the crash levels, while the larger wavenumbers ($k > 0.15 \text{ cm}^{-1}$) still have increased power. This indicates that, even after the transmission enhancement of the injection source subsides, there is still power cascading to larger wavenumbers. Finally, in the last time window, 0.525 to 0.875 ms, the spectrum has returned to "before" the crash power levels. Throughout this article, we have chosen to present data at $r/a \sim 0.81$ because its value of $k_{d\parallel}$ is near the average of $k_{d\parallel}$ values in Fig. 4 (neglecting the value near the wall). The effects seen in Fig. 6 occur at all positions though.

This sequence of events corresponds with the well-documented evolution of magnetic mode activity during the sawtooth crash, shown in Fig. 2. The buildup of power in the smallest wavenumbers occurs while the $(m, n) = (1, > 6)$ tearing mode amplitudes are increasing. The elevated power at all wavenumbers corresponds to the time at which the $(m, n) = (0, 1)$ tearing mode amplitude is the largest and non-linearly couples to the $(m, n) = (1, > 6)$ tearing modes. When the $(m, n) = (0, 1)$ tearing mode has decreased to the point where it is no longer the dominant mode amplitude, the entire spectrum is back to "before" the crash power levels. This sequence confirms that it is appropriate to use a model based on power cascading from small wavenumbers to larger wavenumbers to describe the spectrum. The spectra have a hybrid power law-exponential character at all times.

Furthermore, although it is shown in Fig. 6 that the power

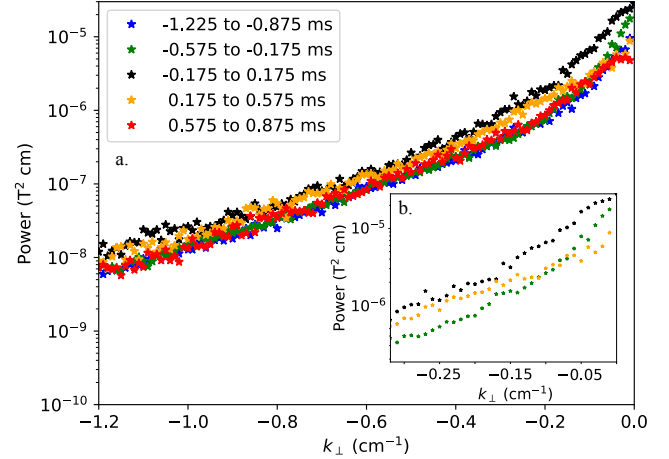


FIG. 6. a.) The k_{\perp} power spectrum in the time ranges -1.225 to -0.875 ms (blue stars), -0.525 to -0.175 ms (green stars), -0.175 to 0.175 ms (black stars), 0.175 to 0.525 ms (orange stars), and 0.525 to 0.875 ms (red stars), all relative to the crash, are compared. b.) Enhanced view of the -0.525 to -0.175 ms (green stars), -0.175 to 0.175 ms (black stars), and 0.175 to 0.525 ms (orange stars) k_{\perp} power spectra. [Associated dataset available at <http://dx.doi.org/10.5281/zenodo.4455538>] (Ref. 29).

in the spectrum increases at all wavenumbers during the crash, the general shapes of the "before" and "during" spectra are not drastically different. Both fall off more than a typical power-law. This indicates there is a well-developed cascade at all times regardless of the plasma condition. It is likely that the $(m, n) = (1, > 6)$ tearing modes are always providing power to be cascaded to larger wave numbers. The cascade is then only enhanced by the sawtooth crash through the non-linear coupling with $(m, n) = (0, 1)$ and anomalous viscosity.

This enhancement feature is similar to another phenomenon in MST plasmas, involving anomalous ion heating and particle energization. As mentioned in Section I, there has been a large effort to describe the anomalous features of ion heating and particle energization during the sawtooth crash, but the anomalously high ion temperatures and non-Maxwellian tails in particle distribution functions exist throughout the discharge. These features are only enhanced by the sawtooth crash. This suggests there may be a connection between dissipation, anomalous ion heating and particle energization. There have been previous attempts to connect magnetic fluctuations to particle heating in MST plasmas via ion cyclotron resonance,^{22,23,34,35} where energy is dissipated through an ion cyclotron resonance. Though this model seemed promising, it did not take into account all of the heating observations.³⁶ The measurements of k_d indicate the dissipation is not likely to be collisional, both in the lack of a spatial dependence reflecting $T_e(r)$ and in the magnitude of k_d . The onset is roughly at the lower end of the ion cyclotron frequency range when considering minority ions.

It is instructive to relate the intrinsically time-dependent behavior of the spectrum following the sawtooth crash to the

steady-state spectrum of Eqs. 1 and 3 used to infer the properties of fluctuation dissipation. While the latter assumes a time invariant cascade process and therefore cannot capture the transient features of Fig. 6 it nonetheless is consistent with Fig. 6 in an important and notable manner. As shown in Ref. 18, b , $\alpha > 0$ indicate that the inertial range is at lower k and the dissipation range is at higher k , as concluded from the analysis of Fig. 6. Positive values for b and α were generated from the fit of Figs. 3 and 5 to stationary data. Though not shown, negative values of b and α , which actually characterize ion temperature gradient turbulence in gyrokinetic simulations, are very far from matching the data.

V. CONCLUSION

Dissipation in magnetic wavenumber spectra during magnetic reconnection has been characterized both spatially and temporally. A novel probe with multiple magnetic pickup coils is used to measure magnetic field dynamics at the edge of MST RFP plasmas during magnetic reconnection events. Using signals from different combinations of coils enables multiple measurements of the spectral density, which are ensembled to decrease uncertainty of the wavenumber spectrum. The k_{\perp} power spectrum measured at $r/a \sim 0.81$ exhibits power-law plus exponential behavior, with a $k_d = 0.85 \text{ cm}^{-1}$.

The probe is inserted at different locations near the edge of the plasma to sample possible changes in the spectrum due to a dependence on the density and temperature, which would be expected for collisional dissipation. The calculated wavenumber spectrum at each depth exhibits a power-law and exponential fit, agreeing with previous measurements and indicating the spatially consistent occurrence of dissipation. The values of k_d dissipation are not consistent with classical resistivity or viscosity, but they do correspond well to anomalous viscosity inferred from flow damping measurements. This suggests a common mechanism is responsible for both dissipation of magnetic fluctuations and anomalous viscosity.

The fine temporal resolution of the measurements shows that the spectrum is most likely energized by long-wavelength tearing modes. A transient enhancement in the tearing band of frequencies that lasts about one eddy turnover time is detected at the abrupt sawtooth crash. No other deviations from a spectrum well fit by a dissipative cascade are observed.

ACKNOWLEDGMENTS

The authors would like to thank Steve Oliva for the SolidWorks model of MST. We would also like to thank Mat Leeds for his help constructing and characterizing the *millimeter probe*. This work was supported by the U. S. Department of Energy Office of Science, Office of Fusion Energy Sciences program, under the Awards DE-FG02-97ER54417, DE-FC02-05ER54814, DE-SC0018266, and DE-FG02-85ER53212.

DATA AVAILABILITY STATEMENT

The data that support the findings of this study are openly available in Zenodo at <http://doi.org/10.5281/zenodo.4455538> (Ref. 29).

REFERENCES

- ¹R. N. Dexter, D. W. Kerst, T. W. Lovell, S. C. Prager, and J. C. Sprott, *Fusion Technol.* **19**, 131 (1991).
- ²J. W. Belcher and L. Davis Jr., *J. Geophys. Res.* **76**, 3534 (1971).
- ³C. C. Chaston, C. Salem, J. W. Bonnell, C. W. Carlson, R. E. Ergun, R. J. Strangeway, and J. P. McFadden, *Phys. Rev. Lett.* **100**, 175003 (2008).
- ⁴G. D. Conway, *Plasma Phys. Control. Fusion* **50**, 124026 (2008).
- ⁵S. A. Balbus and J. F. Hawley, *Rev. Mod. Phys.* **70**, 1 (1998).
- ⁶G. Fiksel, A. F. Almagri, B. E. Chapman, V. V. Mirnov, Y. Ren, J. S. Sarff, and P. W. Terry, *Phys. Rev. Lett.* **103**, 145002 (2009).
- ⁷W. X. Ding, D. L. Brower, G. Fiksel, D. J. Den Hartog, S. C. Prager, and J. S. Sarff, *Phys. Rev. Lett.* **103**, 025001 (2009).
- ⁸R. J. Leamon, C. W. Smith, N. F. Ness, W. H. Matthaeus, and H. K. Wong, *J. Geophys. Res.* **103**, 4775 (1998).
- ⁹C. W. Smith, K. Hamilton, B. J. Vasquez, and R. J. Leamon, *Astrophys. J. Lett.* **645**, L85 (2006).
- ¹⁰C. S. Salem, G. G. Howes, D. Sundkvist, S. D. Bale, C. C. Chaston, C. H. K. Chen, and F. S. Mozer, *Astrophys. J. Lett.* **745**, L9 (2012).
- ¹¹L. Marrelli, P. Martin, M.E. Puiatti, J.S. Sarff, B.E. Chapman, J.R. Drake, D.F. Escande, and S. Masamune, *Nucl. Fusion* **61**, 023001 (2021).
- ¹²Y. Ren, A. F. Almagri, G. Fiksel, S. C. Prager, J. S. Sarff, and P. W. Terry, *Phys. Rev. Lett.* **107**, 195002 (2011).
- ¹³D. J. Thuecks, A. F. Almagri, J. S. Sarff, and P. W. Terry, *Phys. Plasmas* **24**, 022309 (2017).
- ¹⁴Ellen G. Zweibel and Masaaki Yamada, *Annu. Rev. Astron. Astrophys* **47**, 291 (2009).
- ¹⁵I. H. Hutchinson, M. Malacarne, and P. Noonan, *Nucl. Fusion* **24**, 59 (1984).
- ¹⁶S. Choi, D. Craig, S. C. Prager, *Phys. Rev. Lett.* **96**, 145004 (2013).
- ¹⁷N. A. Crocker, G. Fiksel, S. C. Prager, and J. S. Sarff, *Phys. Rev. Lett.* **90**, 035003 (2003).
- ¹⁸P. W. Terry, A. F. Almagri, G. Fiksel, C. B. Forest, D. R. Hatch, F. Jenko, M. D. Nornberg, S. C. Prager, K. Rahbarnia, Y. Ren, and J. S. Sarff, *Phys. Plasmas* **19**, 055906 (2012).
- ¹⁹S. Gangadhara, D. Craig, D. A. Ennis, D. J. Den Hartog, G. Fiksel, and S. C. Prager, *Phys. Plasmas*, **15**, 056121 (2008).
- ²⁰S. T. A. Kumar, A. F. Almagri, D. Craig, D. J. Den Hartog, M. D. Nornberg, J. S. Sarff, and P. W. Terry, *Phys. Plasmas* **20**, 056501 (2013).
- ²¹M. S. Cartolano, D. Craig, D. J. Den Hartog, S. T. A. Kumar, and M. D. Nornberg, *Phys. Plasmas*, **21**, 012510 (2014).
- ²²E. Scime, S. Hokin, N. Mattor, C. Watts, *Phys. Rev. Lett.* **68**, 2165 (1992).
- ²³E. Scime, M. Cekic, D. Den Hartog, S. Hokin, D. Holly, and C. Watts, *Phys. Fluids B* **4**, 4062 (1992).
- ²⁴R. Magee, D. DenHartog, S. T. A. Kumar, A. F. Almagri, B. Chapman, G. Fiksel, V. Mirnov, E. D. Mezonlin, and J. Titus., *Phys. Rev. Lett.* **107**, 6 (2011).
- ²⁵J. B. Titus, E. D. Mezonlin, and J. A. Johnson, III., *Phys. Plasmas* **21**, 062511 (2014).
- ²⁶A. M. DuBois, A. F. Almagri, J. K. Anderson, D. J. Den Hartog, J. D. Lee, J. S. Sarff, *Phys. Rev. Lett.* **118**, 075001 (2017).
- ²⁷J. S. Sarff, A. F. Almagri, J. K. Anderson, M. Borchardt, W. Cappechi, D. Carmody, K. Caspary, B. E. Chapman, D. J. Den Hartog, J. Duff *et al.*, *Nucl. Fusion* **55**, 104006 (2015).
- ²⁸J. M. Beall, Y. C. Kim, and E. J. Powers, *J. Appl. Phys.* **53**, 3933 (1982).
- ²⁹J. B. Titus. (2021). Dissipation in the Magnetic Turbulence of Reversed Field Pinch Plasmas Figure Data [Data set]. Zenodo. <http://doi.org/10.5281/zenodo.4455538>
- ³⁰B.E. Chapman, A. F. Almagri, J. K. Anderson, T. M. Biewer, P. K. Chattopadhyay, C.-S. Chiang, D. Craig, D. J. Den Hartog, G. Fiksel, C. B. Forest *et al.*, *Phys. Plasmas* **9**, 5 (2002).

- ³¹Y. L. Ho and G. G. Craddock, *Phys. Fluids B* **3**, 721 (1991).
- ³²P. W. Terry and V. Tangri, *Phys. Plasmas* **16**, 082305 (2009).
- ³³A. F. Almagri, J. T. Chapman, C. S. Chiang, D. Craig, D. J. Den Hartog, C. Hegna, and S. C. Prager, *Phys. Plasmas* **5**, 3982 (1998).
- ³⁴N. Mattor, P. W. Terry, and S. C. Prager, *Comments on Plasma Phys. and Contr. Fusion* **15**, 65 (1992).
- ³⁵V. Tangri, P. W. Terry, and G. Fiksel, *Phys. Plasmas* **15**, 11 (2008).
- ³⁶R. M. Magee, Ph.D. thesis, University of Wisconsin-Madison, 2011.
- ³⁷J. J. Sakurai, *Modern Quantum Mechanics* (Addison-Wesley, 1994).
- ³⁸J. Gea-Banacloche, *Am. J. Phys.* **67**, 776 (1999).
- ³⁹K. Zhukovsky and G. Dattoli, *Applied Mathematics and Computation* **217**, 7966 (2011).
- ⁴⁰M. V. Berry and N. L. Balazs, *Am. J. Phys.* **47**, 264 (1979).
- ⁴¹J. Broky, G. A. Siviloglou, A. Dogariu, and D. N. Christodoulides, *Opt. Express* **16**, 12880 (2008).
- ⁴²G. A. Siviloglou, J. Broky, A. Dogariu, and D. N. Christodoulides, *Phys. Rev. Lett.* **99**, 213901 (2007).
- ⁴³G. A. Siviloglou and D. N. Christodoulides, *Opt. Lett.* **32**, 979 (2007).
- ⁴⁴S. Chávez-Cerda, U. Ruiz, V. Arrizón, and H. M. Moya-Cessa, *Opt. Express* **19**, 16448 (2011).
- ⁴⁵T. Vettenburg, H. I. C. Dalgarno, J. Nylk, C. Coll-Lladó, D. E. K. Ferrier, T. Čížmár, F. J. Gunn-Moore, and K. Dholakia, *Nature Methods* **11**, 541 (2014).
- ⁴⁶N. Voloch-Bloch, Y. Lereah, Y. Lilach, A. Gover, and A. Arie, *Nature* **494**, 331 (2013).
- ⁴⁷J. E. Avron and H. I. W, *Communications in Mathematical Physics* **52**, 239 (1977).
- ⁴⁸L. F. Matin, H. H. Bouzari, and F. Ahmadi, *Journal of Theoretical and Applied Physics* **8**, 140 (2014).
- ⁴⁹U. Leonhardt, *Measuring the Quantum State of Light* (Cambridge Studies in Modern Optics, 1997).
- ⁵⁰M. Abramovitz and I. Stegun, *Handbook of Mathematical Functions* (Dover, 1964).
- ⁵¹V. V. Nesvizhevsky, H. G. Börner, A. K. Petukhov, H. Abele, S. B. Ier, F. J. Rueß, T. Stöferle, A. Westphal, A. M. Gagarski, G. A. Petrov, and A. V. Strelkov, *Nature* **415**, 297 (2002).
- ⁵²J. H. Eberly, N. B. Narozhny, and J. J. Sanchez-Mondragon, *Phys. Rev. Lett.* **44**, 1323 (1980).
- ⁵³A. Torre, *Journal of Optics* **17**, 075604 (2015).
- ⁵⁴J. D. Ring, J. Lindberg, A. Mourka, M. Mazilu, K. Dholakia, and M. R. Dennis, *Opt. Express* **20**, 18955 (2012).
- ⁵⁵F. Soto-Eguibar and H. M. Moya-Cessa, *Rev. Mex. Fís. E* **59**, 122 (2013).
- ⁵⁶M. A. Bandres, I. Kaminer, M. Mills, B. Rodríguez-Lara, E. Greenfield, M. Segev, and D. N. Christodoulides, *Opt. Photon. News* **24**, 30 (2013)

